# Intensification of catalytic $CO_2$ methanation mediated by *in-situ* water removal through a high-temperature polymeric thin-film composite membrane

Sara Escorihuela[a†], Cristina Cerdá-Moreno[a†], Fynn Weigelt[b†], Sonia Remiro-Buenamañana[a], Sonia Escolástico[a], Alberto Tena[b,c], Sergey Shishatskiy[b], Torsten Brinkmann[b], Antonio Chica[a], Jose M. Serra[a]

[a.] *Instituto de Tecnología Química, Universitat Politècnica de València-Consejo Superior de Investigaciones Científicas, Avda. Los Naranjos, s/n, 46022, Valencia, Spain.*

[b.] *Helmholtz-Zentrum Hereon, Institute of Membrane Research, Max-Planck-Str.1, 21502 Geesthacht, Germany.*

[c.] *European Membrane Institute (EMI) Twente, University of Twente, Drienerlolaan 5, 7522 NB Enschede, The Netherlands.*

† Authors contributed equally.

Catalytic $CO_2$ methanation technology can be improved by process intensification, i.e. enabling higher energy efficiency and process sustainability. Here, thin-film composite membranes (TFCM) were developed for *in-situ* water removal in a catalytic membrane reactor (CMR) for the Sabatier process. The selective separation layer (1.4µm-thick) of the composite membrane is made of the polyimide 6FDA-6FpDA, a glassy polyimide, which exhibits high permeability and selectivity together with stable function at unprecedented high temperatures (>200 °C), compared to polyimides reported until now (90 °C), thus matching the temperature range of Sabatier reactors. Remarkably, TFCM developed in this work, allow to extract an outstanding amount of water up to 1 $m^3/(m^2 \cdot h \cdot bar)$ at 260 °C. TFCM was implemented for the water removal from the methanation reaction in a CMR operated at 260 °C and using Ni-Todorokite as catalyst. The TFCM-mediated water-extraction enabled to raise both catalytic stability and activity during CMR operation. $CO_2$ conversion stability was greatly improved exhibiting a conversion value of 72 % during the course of the reaction (21 % increase in $CO_2$ conversion), with a water removal of 12.5 % and specific flux of ~100 $g \cdot h^{-1} \cdot m^{-2}$.

## 1. Introduction

Global warming, energy shortage and pollution have led global efforts of science and technology research towards clean and efficient energy systems. In recent years, different strategies have emerged to reduce carbon dioxide ($CO_2$) emissions such as its capture and storage, or its use to store renewable energy via hydrogenation to produce fuels and other molecules of interest.[1,2] The development of these processes is essential to mitigate climate change and to achieve the aims set out in the Paris Agreement,[3] which establishes the objective of maintaining the global average temperature increase below 2 °C above pre-industrial levels.

The possibility of using $CO_2$ as feedstock for fuels and chemicals production by reducing $CO_2$ to methane ($CH_4$), known as Sabatier reaction [4] (Equation (1)), is currently considered as one of the most attractive alternatives.[5–7] This exothermic process uses molecular hydrogen ($H_2$) which, in principle, could be provided by the energy surplus from renewable sources, while $CH_4$ could be used as an energy carrier easily transported through the current gas pipelines network. The $CO_2$ availability is an important consideration related to the economy of the methanation process. For instance, the use of biogas as $CO_2$ source is an interesting option, since its direct conversion without separation would increase $CH_4$ concentration in the final outlet gas stream, boosting its energetic value and improving the global economy of the biogas production process.

$CO_2$ hydrogenation (Equation 1) is a linear combination of reverse water-gas shift reaction and carbon monoxide (CO) methanation (Equation (2) and (3), respectively).

$$CO_2 + 4H_2 \leftrightarrow CH_4 + 2H_2O(g) \qquad \Delta H = -164\ kJ/mol \qquad (1)$$

$$CO_2 + H_2 \leftrightarrow CO + H_2O(g) \qquad \Delta H = 41\ kJ/mol \qquad (2)$$

$$CO + 3H_2 \leftrightarrow CH_4 + H_2O(g) \qquad \Delta H = -206\ kJ/mol \qquad (3)$$

Given the great stability of the $CO_2$ molecule, the use of catalysts as well as temperatures above 250 °C are essential in order to achieve acceptable conversion and selectivity values. Hydrogenation of $CO_2$ to $CH_4$ has been investigated using catalytic systems based on supported VIII group metals on various supports.[8–11] Among these catalysts, Ni-based catalysts have been widely employed for the $CO_2$ methanation reaction due to their high catalytic activity and high methane selectivity.[12–14]

However, it is known that conventional Ni-based catalysts suffer from severe catalyst deactivation during this reaction mainly due to two reasons: (i) the sintering of nickel particles,[15] which could be mitigated by the addition of a second metal such Fe, Sm, Ce, La, Mg, and Y, that would enhance the stability and catalytic activity of Ni-based catalysts;[16–21] and (ii) at low temperature, the interaction of the metal particles with CO, the formation of carbon deposits and mobile nickel subcarbonyls.[22] The necessity to develop more efficient technologies to produce $CH_4$ from $CO_2$ reduction processes is clear. One way of enhancing the reaction performance, is shifting the equilibrium. It is worth noting that the Sabatier reaction is not thermodynamically limited at 260 °C and 1 bar, however it is kinetically limited.[9] $CO_2$ methanation can be enhanced using water sorbents such as zeolites, $La_2O_3$ or CaO.[23,24] According to the Le Chatelier principle, the yield and selectivity of the targeted compound are boosted by the removal of the byproducts of the reaction.[25] An option in this process is to shift the equilibrium by eliminating water. Water removal is important in several industrial applications since it is a byproduct in several chemical reactions. In this way, Gao et al. improved the $CH_4$ yield by using a water sorption catalyst, Ni-zeolite 5A.[26] The adsorption of $H_2O$ in the zeolite, resulted in $CH_4$ yield increase, reaching values of 100 %.

However, as main drawbacks to be considered, adsorbents need to be regenerated once they reach saturation, together with the added complication of selective separation when the reaction is heterogeneously catalysed. In addition, as water sorption is favoured thermodynamically at low temperature, the development of materials capable of retaining water at high temperatures is challenging.

An alternative to absorbents is to carry out the extraction from water directly from the reaction from the vapour phase. Such an alternative is offered by the use of catalytic membrane reactors (CMR). Membranes and CMR have gained intensive attention of researchers around the world due to their extensive number of applications.[27,28,29,30,31,32]

The integration of a water selective membrane in a catalytic reactor enables the process intensification concept which leads to higher energy and carbon-use efficiency. These membranes are able to provide (i) effective purification of a desired reaction product; (ii) distributed and controlled dosing of one reactant; and (iii) optimal removal of products that could deactivate or poison the catalyst or limit the equilibrium conversion dictated by thermodynamics.[33,34]

However, some of the processes, such as the methanation reaction explained before, are extremely challenging. The process conditions are extreme for polymeric materials such the combination of high feed pressures and very high temperatures. Under those conditions, the main part of the membrane materials will degrade and lose their performances. Therefore, the design of highly stable components is critical in order to ensure stable performances over the time.

Polymeric membranes, as dense membranes, follow a solution-diffusion model. Permeability can be expressed as the product of diffusion coefficient and solubility coefficient. Diffusion coefficient is related with the kinetics and it is related to the mobility of the individual molecules in the membrane material (molecular size). On the other hand, solubility coefficient is an equilibrium term and it is associated to the number of molecules dissolved in the material (molecular interaction). Several polymers showed a preferential interaction or transport towards water vapour. A clear example are the polyethylene glycol-based polymers, such as PolyActive or Pebax, that show very high water vapour fluxes. However, the amount of polymeric membranes tested at temperatures above 200 °C is very limited.[35–37]

Polymers such as sulfonated polyether ketone (SPEEK) due to the interaction between the water vapour and the sulfonate groups present in the polymer chain, shows very high water permeability and great $H_2O/N_2$ selectivity.[38] However, this type of materials present a severe thermal degradation at temperatures above 200 °C under inert atmosphere.[39]

Combining the elevated pressures and temperatures, the amount of polymeric materials tested are negligible. Polybenzimidazole (PBI) combines a very high thermal resistance and a preferential interaction between the polymer chain and the water vapour. Although this material has been already tested at very elevated temperatures, its main drawbacks are the relatively low permeability and limited processability due to very high brittleness.[40,41]

In similar way, polyimides exhibit superior separation performance, permeability and selectivity than other glassy polymers, well-balanced thermal and chemical stability, and processability, hence, they have been thoroughly investigated in the last 40 years.[42,43] A broad variety of works related to polyimides, as well as several reports regarding outstanding polyimide properties, have been published,[44] but only few of the documented polyimides proved to be stable at temperatures around 100 °C. In fact, the highest temperatures reported are in the range from 60 to 90 °C and very few reported water permeation.[45–50]

Thin-film composite membrane (TFCM) for the *in-situ* water separation in the methanation reaction has been developed in this work. Methanation reaction was performed at 260 °C using Ni-Todorokite as catalyst. The reaction has been evaluated with and without the developed water selective membrane, full characterization is also presented. The results show that the extraction of water not only improves the reaction yield but also the catalytic performance when a TFCM was employed.

## 2. Experimental

### 2.1. Materials

$MnCl_2{\cdot}4H_2O$, $Ni(NO_3)_2{\cdot}6H_2O$ and $KMnO_4$ were provided by Sigma-Aldrich (Darmstadt, Germany) and NaOH was provided by Scharlab (Barcelona, Spain). Dimethyl acetamide, tetrahydrofuran (THF) and toluene were purchased from Merck GmbH (Darmstadt, Germany). 3M™ Fluorinert™ FC-770 > 99 % was purchased by IOLITEC Ionic Liquids Technologies GmbH (Heilbronn, Germany).

Polybenzimidazole (PBI), a Poly[2,2'-(m-phenylene)-5,5'-bibenimidazole], was purchased from PBI® performance products, Inc. (Charlotte, USA) as solution in dimethylacetamide (DMAc). Polyethylene glycol (PEG) was acquired from Sigma-Aldrich with an average molecular weight of 2000 g/mol. Monomers for polyimide synthesis are 4,4'-(hexafluoroisopropylidene) diphthalic anhydride (6FDA) and 2,2-bis(4-aminophenyl) hexafluoropropane (6FpDA) which were purchased from Sigma-Aldrich (St. Louis, USA). Teflon® AF 2400 was purchased from E. I. du Pont de Nemours (Wilmington, USA).

**Catalyst**

The Ni Todorokite catalyst was synthesized according to the procedure described by Onda et al.[51]
Todorokite is a type of octahedral molecular sieve (OMS) which is known as OMS-1. It is composed of octahedral $MnO_6^{x-}$ ions forming tunnels of 6.9x6.9x9.76 Å with three manganese oxide octahedrons on each side.[52] This material shows high catalytic activity compared to other type of supported catalysts probably due to its capability to activate $CO_2$ via a dissociative as well as an associative mechanism.[53] This finding supports the use of this catalyst in the present study.
Catalyst was firstly reduced with pure $H_2$ at 450 °C for 2 h in an external oven. When the reduction oven was at room temperature, the catalyst was subjected to a passivation process with air and inert gas ($N_2$). This process aims to preserve the reduced state of the catalyst during the transfer to the methanation chamber. It consists of a surface passivation of reduced metal particles by controlled re-oxidation to create a thin and protective oxide layer.[54,55]

**Thin-film composite membrane (TFCM)**
The selective water vapor removal during the $CO_2$ methanation reaction was performed with a TFCM composed of polyphenylene sulphide (PPS) as a non-woven support, polybenzimidazole (PBI) as a porous support, a selective dense layer of a highly thermally stable polymer, the polyimide 6FDA-6FpDA, and Teflon® AF 2400 as a protective layer that will increase durability, and sealing layer as it corrects small defects that may be produced in the membranes.
Non-woven polyphenylene sulphide (PPS) was selected due to its excellent thermal and chemical resistance and high porosity. Polyimide 6FDA-6FpDA was synthesized for the current work using the monomers 4,4'-(hexafluoroisopropylidene) diphthalic anhydride (6FDA) and 2,2-bis(4-aminophenyl) hexafluoropropane (6FpDA), following the classical *in-situ* silylation two steps method.[56] A detailed description of this synthesis can be found in a previous work.[57] PBI porous support on PPS non-woven was prepared on a lab scale membrane casting machine. The process can be found in previous work.[58] TFCMs of 6FDA-6FpDA were prepared by dip coating process. First, the porous support was dipped into toluene in order to fill the pores and allowed to dry at ambient conditions to evaporate toluene from the membrane surface but, to keep toluene in the porous structure of PBI. Secondly, the samples were dip coated using the 6FDA-6FpDA solution in THF (3.5 wt. %) and dried at 50 °C. Afterwards, samples were dip coated by 1 wt. % Teflon® AF 2400 solution in FC-770 to get a protective layer out of Teflon® AF 2400 and dried again on the heating plate. TFCMs were subsequently dried in an oven under vacuum for 24 h at 270 °C, in order to avoid aging of the polymer selective layer. It is worth noting that membranes are thermally treated at temperatures above methanation reaction' conditions.

**2.2. Characterization**
**Catalyst**
Crystalline structure of the catalyst was evaluated by X-ray diffraction (XRD) by a PANalytical CUBIX diffractometer with Cu Kα1.2 radiation. The applied current and voltage were 40 mA and 45 kV, respectively. The samples were scanned in the $2\theta$ range from 3.0° to 90.0°.
Temperature programmed reduction (TPR) was carried out to gain insight into the catalyst behaviour in a reductive environment. This analysis was developed using a Micromeritics Autochem 2910 equipped with a TCD detector. The sample (50 mg approximately) was loaded into a quartz reactor and, after being pre-treated with an Ar flow at room temperature for 15 min, the temperature was increased up to 900 °C at a

heating rate of 10 °C/min in a flow of Ar and $H_2$ (50 mL/min, 10 % of $H_2$) while the $H_2$ consumption was monitored.
Chemical composition of the catalyst was determined with a Varian 715-ES ICP-Optical Emission Spectrometer, after solid dissolution using an aqueous solution containing $HNO_3$/HCl/HF.
The textural properties of the catalyst were determined from $N_2$ adsorption isotherms measured at -196 °C in a Micromeritics ASAP 2420. Before the $N_2$ physisorption, the catalyst was degassed at 80 °C for 12 h.
Field-emission scanning electron microscope (FE-SEM) (Zeiss Ultra 55, Oberkochen, Germany), high resolution field-emission scanning electron microscope (HR-FESEM) (Zeiss GeminiSEM 500, Oberkochen, Germany), and high-resolution transmission electron microscope (HR-TEM) (JEM 2100F, Akishima, Tokio, Japan) equipped with an energy dispersive X-ray equipment (EDX), were used for studying the morphology of the samples. Further semi-quantitative analysis of the catalyst was performed by EDX.
X-ray photoelectron spectroscopy (XPS) spectra of the catalyst were recorded with a SPECS spectrometer with a Phoibos 150 MCD-9 multichannel analyzer using a non-monochromatic $MgK_\alpha$ (1253.6 eV) X-Ray radiation. The pass energy and the X-ray power were 30 eV and 100 W, respectively. The sample was pelletized, loaded onto the sample holder and measured at room temperature and a pressure of $10^{-9}$ mbar. Then, the sample was submitted to $H_2$ reduction (15 mL/min) at 450 °C and atmospheric pressure for 2 h in a high-pressure reactor connected under UHV to the XPS analysis chamber. In the case of the catalyst after reaction, the samples were measured directly as powder. XPS spectra were referenced to the C 1s peak (284.5 eV).

**TFCM**
Field-emission scanning electron microscope (FE-SEM) (Zeiss Ultra 55, Oberkochen, Germany), equipped with FIB was used for the structural characterization of the TFCM.

**Permeation test**
Mixed gas measurements at high temperature (from 240 to 260 °C) were performed to obtain permeance values and real selectivities for the TFCM. The employed set-up consists of different mass flow controllers with the possibility to introduce $H_2$ and $CO_2$ as feed gas and Ar as sweep gas. In series with $H_2$ and $CO_2$ mass flow controllers, a gas bubbler allows the introduction of water vapour into the gas stream. Membranes were placed in the centre of the reactor and sealed from both sides. Hence, two well-defined chambers separated by the sample allow to perform measurements at high temperature. 64 mL/min of a stream composed by 62 % $H_2$, 16 % $CO_2$ and 22 % $H_2O$ was used as feed gas and 50 mL/min of Ar were employed as sweep. $H_2$ and $CO_2$ concentrations in the permeate side were measured with a Micro-GC CP-4900 (equipped with a TCD detector and Molsieve 5A and Pora PLOT Q columns) and water vapour was analysed by a hygrometer which controls the relative humidity (RH). RH can be translated into partial pressure of water vapour at the permeate side that acts as driving force of the permeation process.

**Catalytic reactor**
The methanation reactor set-up consists of a micro-reactor with two separated chambers (reaction and permeation chamber) that allows to place the membrane and seal the sample by rubber rings in the centre. More detailed information is given in the supporting information (**Fig. S1**).

Catalytic performance evaluation was divided in two parts:
**(i)** Blank reaction. The aim of this first part is to evaluate the behaviour of the catalyst without the water selective membrane, to compare and normalize the advantages and

improvements when the TFCM is placed in the CMR. A blank catalytic test was performed using an aluminium disc (not permeable) instead of a gas separation membrane and no sweep gas was fed into the permeation chamber.
**(ii)** $CO_2$ methanation with TFCM for *in-situ* water removal. The catalytic methanation test was performed by using the TFCM. In this case, a flow of 30 mL/min Ar was introduced as sweep gas into the permeate chamber.
In both cases, 0.033 g of catalyst were used in the reaction. The catalyst was shaped into granules sized between 0.250 to 0.425 mm. Afterwards, the catalyst was mixed with silicon carbide (SiC) in 1:1 weight ratio and distributed homogenously along the channel of a volume of 100 $mm^3$ and a longitudinal shape. Once the reactor module was perfectly closed and located in the methanation module, a second reduction (employing 15 mL/min of pure $H_2$) was performed at 250 °C for 2 h. Then, temperature in the reactor was set at 260 °C, feed gases were introduced into the catalyst bed, and hence the reaction started. For the methanation reaction, 5 mL/min of a mixture composed by 72 % of $H_2$, 18 % of $CO_2$ and 10 % of $N_2$ (calibrated cylinder) was used as feed into the reaction chamber. $N_2$ was used as internal standard. 30 mL/min of Ar were injected after the reaction chamber to ensure that all the reaction products, as well as the internal standard, reach correctly the gas chromatograph for analysis. Reaction was performed at 260 °C and atmospheric pressure. Reaction was carried out for 48 h at 260°°C at atmospheric pressure.
The water permeating through the membrane was quantified using a hygrometer. Permeating gases, such as $H_2$, and reaction products were analysed with the GC (Varian CP-3800, TCD HayeSep Q and FID MolSieve 13X).
$CO_2$ conversion, as well as $CH_4$ selectivity and yield were calculated according to Equations (4), (5) and (6), respectively.

$$X_{CO_2} = \frac{\chi_{CO_{2\_0}} - \chi_{CO_2}}{\chi_{CO_{2\_0}}} \cdot 100 \quad (4)$$

$$S_{CH_4} = \frac{\chi_{CH_4}}{\chi_{CO_{2\_0}} - \chi_{CO_2}} \cdot 100 \quad (5)$$

$$Y_{CH_4} = \frac{(X_{CO_2} \cdot S_{CH_4})}{100} \quad (6)$$

where $S_{CH_4}$ is the selectivity of $CH_4$ (%), $\chi_i$ are the molar flowrates of the gases, $\chi_{CO_{2\_0}}$ is feed molar flowrate of $CO_2$, $X_{CO_2}$ is the conversion of $CO_2$ (%) and $Y_{CH_4}$ is the yield of $CH_4$ (%).

## 3. Results and discussion

### 3.1. Catalyst

Ni Todorokite- catalyst has been studied by FESEM and HR-TEM. The fresh material shows a sheet-like morphology (**Fig. 1a**) in which small pores appear after reduction. In these pores, a homogeneous Ni nanoparticles distribution is distinguished (**Fig. 1b**). HR-TEM images allow measuring the Ni particle size distribution, being 80 % of these nanoparticles between 3 to 6 nm, whereas punctual (**Fig. 1c**) and linescans (**Fig. 1d-e**) analyses by EDX confirm that these nanoparticles are composed by Ni.

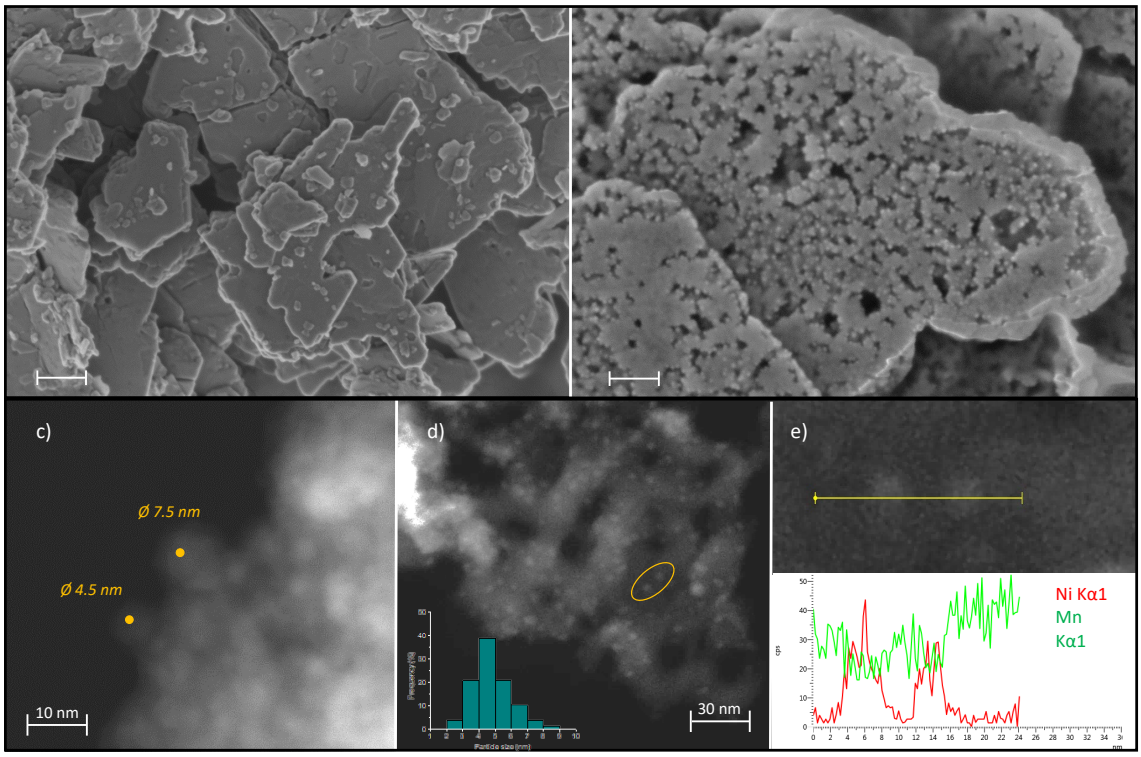


**Fig. 1**. FE-SEM images of fresh catalyst (a) and after reduction (b). HR-TEM images with (c) punctual and (d-e) linescan analysis by EDX.

Chemical composition and textural properties of Ni-Todorokite were measured by ICP and $N_2$ adsorption, respectively. The catalyst contains 50.7 wt. % of manganese and 15.0 wt. % of nickel, and it presents a surface area of 13 $m^2/g$. These results are consistent with the values given by Onda et al. for this kind of materials.[51]

The XRD pattern of the synthesized catalyst Ni-Todorokite is shown in the SI, **Fig. S2**. The main diffraction peaks of the catalyst before reduction are the ones characteristic of the todorokite structure. This todorokite structure is entirely transformed after reduction at 450 °C being MnO the main phase detected while diffraction peaks with low intensity corresponding to metallic nanosized nickel can also be distinguished.

The reducibility of the catalyst was studied by TPR. The profiles of the catalyst before and after the steps of reduction (at 450 °C) and passivation are shown in the SI, **Fig S2**. When the catalyst is previously reduced and passivated, the reduction of the material takes place at a lower temperature as it is ascribed from the intense peak that appears between 180 and 250 °C. Thus, the in-situ reduction can be carried out at these less demanding conditions and, in this way, the properties of the polymeric membrane (with a maximum operation temperature around 280 °C) can be preserved.

Ni-Todorokite catalyst was also evaluated by XPS. **Fig. S3** shows the synthesized and reduced catalyst spectra. Comparing both spectra, the binding energy of the main peak is shifted to lower binding energies indicating that Ni was reduced after $H_2$ treatment.

### 3.2. Selective water removal

In a previous work, the thermal stability of the PBI and the 6FDA-6FpDA polymer was studied by TGA.[58] A single weight loss step was observed at temperatures higher than 450 °C, indicating the high thermal stability of 6FDA-6FpDA. The glass transition temperature ($T_g$) of the 6FDA-6FpDA polymer was 310 °C and the molecular weight ($M_w$) was 190000 g/mol.[57] Regarding PBI support,

the Tg was 427 °C. These values clearly indicate the applicability of the chosen polymers for application in the desired temperature range above 200 °C.

**Fig. 2a** shows FIB micrographs of the TFCM cross-sections. The porous support, the dense 6FDA-6FpDA layer, and the Teflon® AF 2400 protective layer can be observed in the images. Teflon® AF 2400 layer has an irrelevant influence on the permeance of the 6FDA-6FpDA TFCM, as it was observed in previous works.[58] The dense 6FDA-6FpDA layer exhibits a thickness of approximately 1.4 µm. FIB micrographs were recorded after catalytic test completion, hence small surface defects such as the peel-off of the Teflon® AF 2400, may be detected. Nevertheless, it is important to highlight that the membrane has withstood the reaction conditions. **Fig. 2a** presents a cross-section of the porous support composed by PPS and PBI, and a detailed FIB image of the porous support PBI, respectively.

Regarding gas transport properties of TFCMs, permeance values and mixed-gas selectivities were characterized. $H_2$, $CO_2$ and $H_2O$ permeances, as well as $H_2O/H_2$, $H_2O/CO_2$ and $H_2/CO_2$ selectivities were studied. A stream (64 mL/min) composed of 62 % $H_2$, 16 % $CO_2$ and 22 % $H_2O$ was employed as feed gas whereas 50 mL/min of Ar was used as sweep gas, at atmospheric pressure.

**Fig. 2b** shows the permeance of $H_2$, $CO_2$ and $H_2O$ whereas $H_2/CO_2$, $H_2O/H_2$ and $H_2O/CO_2$ real selectivities are plotted in **Fig. 2c**. $H_2O$ permeance shows the highest values, followed by $H_2$ and $CO_2$ which is in concordance with the kinetic diameter: 2.65 Å($H_2O$) < 2.89 Å ($H_2$) < 3.3 Å ($CO_2$). Hence, based on that differences on size, $H_2O/CO_2$ gas pair presents the highest selectivity values, whereas $H_2O/H_2$ exhibits the lowest. At very elevated temperatures, the separation occurs mainly due to the differences on the diffusivity of the different gases. Permeance values slightly increase as a function of temperature in the case of $H_2$ and $CO_2$, while $H_2O$ permeance remains stable with temperature. In general, big differences are found by varying the temperature due to the differences on the solubility and diffusivity. Solubility factor is minimized at temperatures sufficiently elevated, and then the main differences are due to the differences in the diffusion of the gas molecules through the polymeric membrane. Water vapour acts as plasticizer at temperatures lower than 100 $^oC$, which generally it is reflected in a severe increase on the permeance by increasing the temperature. At temperatures above 100 $^oC$, sorption coefficient is lower and this effect is minimized. At very elevated temperatures, as it is shown in **Fig. 2b**, water vapour permeance remains constant, while $H_2$ permeance increases as a result of a higher diffusion coefficient when temperature increases. The increase on the permeance for the $CO_2$ is lower compared to $H_2$ due to the high kinetic diameter. All these facts are reflected in the selectivity. $H_2/CO_2$ selectivity increases as a function of temperature, whereas $H_2O/H_2$ and $H_2O/CO_2$ selectivity decrease, due to the fact that $H_2O$ permeance stays constant.

**Fig. S4** presents a cross-section of the porous support and **Fig. S5** shows a detailed FIB image of the porous support PBI**. Fig. S6** shows the permeance and ideal selectivity values (single gas measurements) of the TFCM for $H_2$ and $CO_2$ from 30 °C to 270 °C. To the best of our knowledge, these values are the highest reported so far, and for this reason, this type of membranes are very promising for water separation in industrial applications.

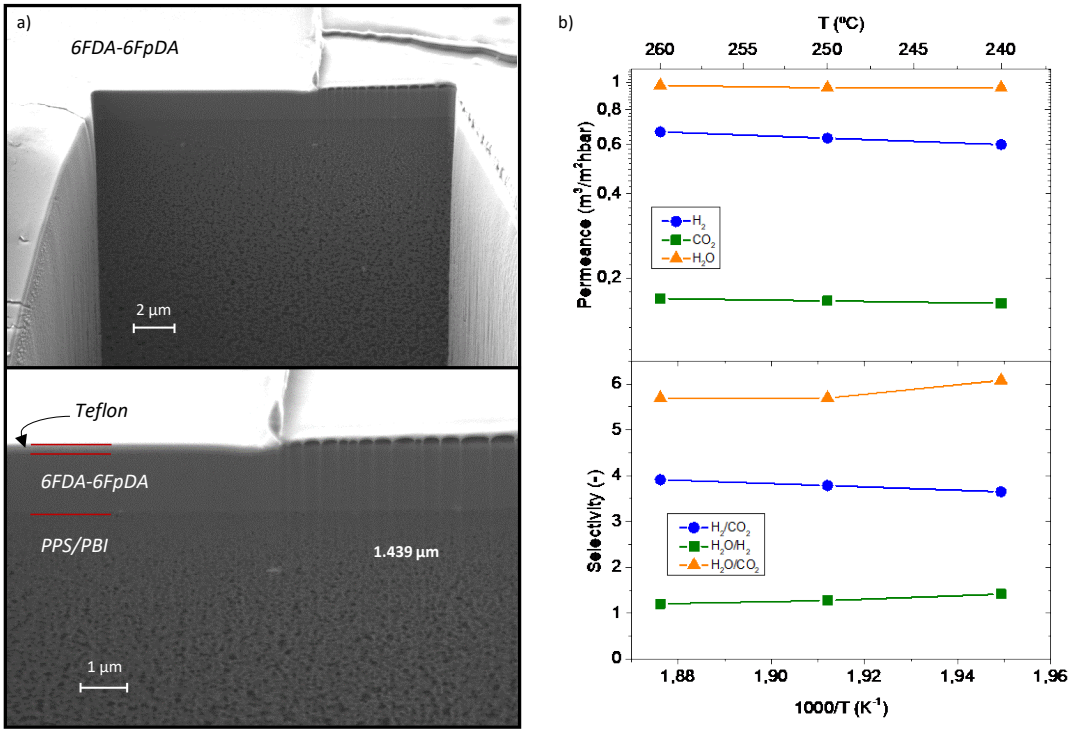


**Fig. 2.** Cross section images from FIB micrographs (a), and gas transport properties of the TFCM (b): $H_2$, $CO_2$ and $H_2O$ permeances and $H_2/CO_2$, $H_2O/H_2$ and $H_2O/CO_2$ selectivities

### 3.3. Catalytic membrane reactor

The study of the catalytic performance is divided in two parts: (i) blank reaction, i.e. methanation reaction without TFCM and (ii) $CO_2$ methanation with TFCM for *in-situ* water removal, see section 2.2 for further experimental details on the catalytic reactor. **Fig. 3a** shows the $CO_2$ conversion as a function of time on stream for both, without (solid symbols) and with TFCM (open symbols). Regarding the experiment without membrane $CO_2$ conversion continuously decreased from 72 % to 61 %, as well as $CH_4$ yield, remaining $CH_4$ selectivity constant at 100 %.

With regard to the CMR experiment, $CO_2$ conversion remains constant as a function of time for the first 24 h. As in the previous experiment, $CH_4$ selectivity was 100 %. During the first 24 h, it was observed that $H_2$ was also permeating through the membrane in agreement with the previous permeation measurements (**Fig. 2**). Note that this $H_2$ permeation to the permeate chamber provokes a $H_2/CO_2$ ratio lower than 4 (ratio employed in the experiment without membrane). Thus, $H_2$ was injected to the permeate chamber to equilibrate the $H_2$ partial pressure across the membrane and, subsequently to avoid the $H_2$ permeation through the membrane. In addition, Ar flow was decreased in order to keep the gas flow rate in the permeation chamber constant. Avoiding the loss of $H_2$ as reactant from the reaction chamber results in an increase of $CO_2$ conversion. After approximately 24 h, $H_2$ was removed from the sweep gas and a drop in the $CO_2$ conversion was observed, in line with the values reached during the first 24 h on stream. $CO_2$ conversion remained constant for another 24 h. It should be noted that the reaction was stable for just under 3 days, obtaining a $CO_2$ conversion of 72 % and, remarkably, 21 % higher than the one obtained without the water-selective membrane.

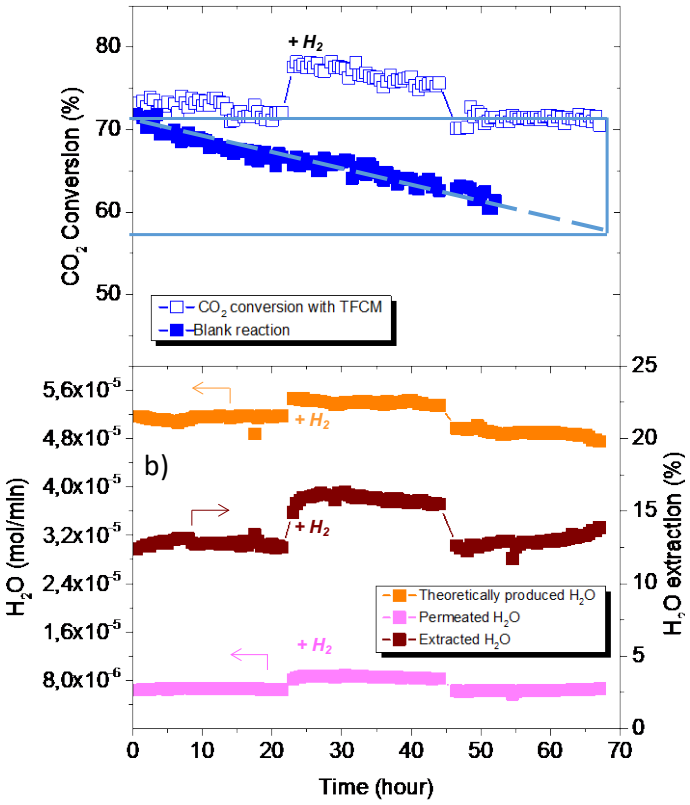


**Fig. 3**. $CO_2$ conversion (%) for the blank reaction (filled symbols) and for $CO_2$ methanation with TFCM (open symbols) (a), Molar flowrate of water production and water permeation (left-y axis) and percentage of water extraction (right-y axes) as a function of time (b).

**Fig. 3b** shows the molar flowrate of theoretically produced $H_2O$ in the reaction chamber and molar flow rate of $H_2O$ permeated through the TFCM, reaching values fluxes of ~100 $g \cdot h^{-1} \cdot m^{-2}$. The TFCM allows to extract the 12 % of the $H_2O$ produced in the methanation reaction. This extraction increases even more, reaching the 15 %, when $H_2$ is added in the sweep chamber. This effect is due to the fact that the decrease of $H_2$ permeation gives rise to an increase of the $CH_4$ production and subsequently in the $H_2O$ production. Hence, the resulting higher $H_2O$ partial pressure gradient through the membrane boosts the $H_2O$ permeation.

Remarkably, it can be concluded that $H_2O$ extraction practically avoids catalyst deactivation, as inferred from the high stability of $CO_2$ conversion and $CH_4$ yield over time. Note that the absolute values of extracted $H_2O$ flow rate were achieved for the system proposed here with 1.4 microns thick membrane. However, reaching lower thickness values of around 100 nm -usual in commercial membranes- will lead to a 10-fold improvement of the $H_2O$ flux, and this would bring much higher percentage of water removal.

As previously mentioned, the Sabatier reaction is not thermodynamically limited at 260 °C and 1 bar, however, it is kinetically limited.[9] In the present work, two effects are observed: (i) increase of the $CH_4$ yield upon *in-situ* $H_2O$ extraction, and (ii) improvement of the catalyst stability. The increase of the $CH_4$ yield can be ascribed to two kinetic effects directly affecting the reaction pathway: (a) regarding the reaction driving force, $H_2O$ removal alleviates the dilution effect and raises the partial pressure of the main reactants; and (b) regarding the adsorptive term, the lower $H_2O$ partial pressure leads to the lower surface coverage of $H_2O$ of the distinct active sites participating in the reaction mechanism, and thus, alleviating the competitive adsorption with the reactants, in line with previous reports.[26,59] Additionally, the use of TFCM enables the constant water extraction from the reaction chamber at a high temperature, which is required for

methanation reaction, and with no need of regeneration as compared with the $H_2O$ adsorption by using zeolites. [26]

Regarding the deactivation of the catalyst in the reaction without $H_2O$ separation membrane, it can be due to the formation of Ni-hydroxide induced by the water formed in the reaction as it has been reported recently.[60] The formation of Ni-hydroxide provokes the decrease of the number of active catalytic sites (metallic particles of Ni) as a consequence of the sintering of Ni particles and the formation of other inactive (oxidized) species. Then, the extraction of water from the reaction chamber helps in supressing this deactivation mechanism. In addition, catalysts subjected to the catalytic tests (blank reaction and $CO_2$ methanation reaction) were studied by XPS and HR-FESEM. XPS results were inconclusive as the Ni particles were partially re-oxidized when the samples were exposed to air before the XPS measurements, as can be ascertained from the XPS spectra plotted in **Fig. S3. Fig. 4a** and **b** show the micrographs of the catalyst employed in the blank test whereas **Fig. 4c** and **d** belong to the $CO_2$ methanation reaction with the selective membrane (after almost 3 days on stream). Ni particles of the catalyst employed in the blank test (**Fig. 4b)** seem to be embedded in the Mn structure, whereas in the catalyst employed in the reaction using TFCM (**Fig. 4d**), Ni particles are better dispersed, more abundant and defined on the pores of the Mn sheet-like morphology. This fact could be associated to the higher activity and stability of the catalyst under *in-situ* water mode.

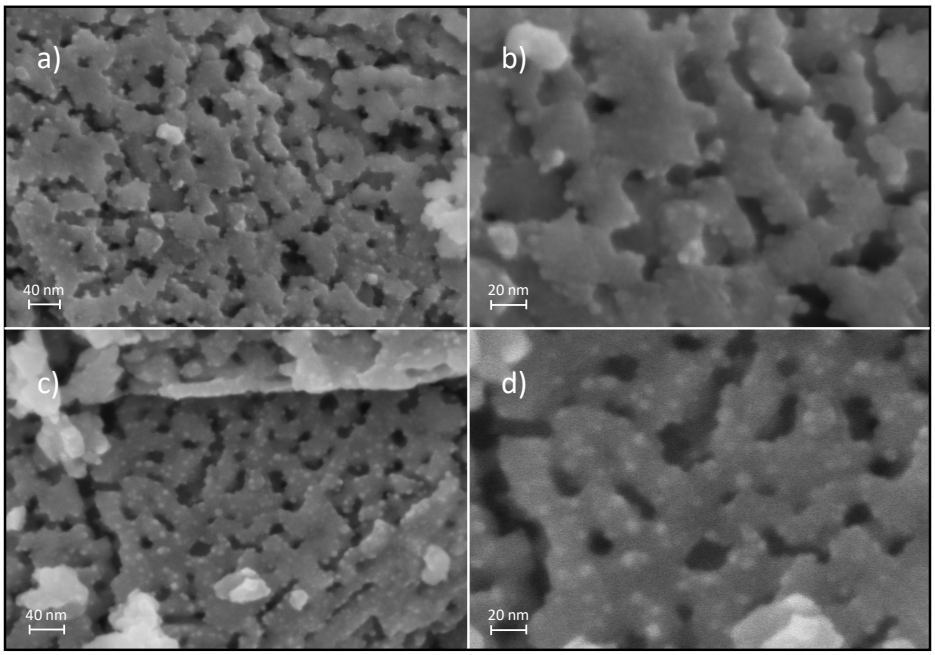


**Fig. 4**. HR-FESEM images of the catalyst used in the blank reaction test (with no membrane) (a,b).and used in the $CO_2$ methanation reaction (with water-selective membrane) (c,d).

**Conclusions**

A catalytic membrane reactor (CMR) composed by (i) a micro-reactor with two chambers, which offers an excellent control of mass and heat transfer rates than other types of reactor,[61] and (ii) a highly-thermally resistant and selective water-separation thin-film composite membrane (TFCM) were developed for operation at 260 °C. TFCM is composed by polyphenylene sulfide (PPS) as a non-woven support, polybenzimidazole (PBI) as a porous support, a selective dense layer of a highly stable polymer, the polyimide 6FDA-6FpDA, and Teflon® AF 2400 as a protective and sealing layer. The high thermal stability (up to 260 °C) of TFCM developed in this study made possible its implementation in the CMR to perform the methanation reaction using a highly active Ni-Todorokite.

The effect of the *in-situ* water removal on the methanation reaction was evaluated. With this aim, the catalytic performance was tested under two different conditions: (i) blank reaction test, i.e. methanation reaction without membrane and (ii) $CO_2$ methanation test with TFCM for *in-situ* water removal. Regarding the first test, a high $CO_2$ conversion is observed although it continuously decreases as a function of time, from 72 % to 61 % in 48 h.

Regarding the CMR test, the $CO_2$ conversion stability was strongly improved by using a thin film composite membrane for the selective *in-situ* removal of the water vapour. For just under three days, $CO_2$ conversion was stable with a maximum water removal of 15 % of the total produced. The water extraction rate reached ~100 $g \cdot h^{-1} \cdot m^{-2}$ values albeit a substantial raise (10-fold) in flux can be reached by reducing the polyimide-layer thickness down to 0.1 μm, as usually done in industrial membrane manufacture.

In addition, because $H_2$ may also permeate through the membrane, during the second day, $H_2$ was included into the sweep gas in order to avoid $H_2$ removal from the catalyst chamber. Consequently, an increase was observed in both water extraction and $CO_2$ conversion. Finally, $H_2$ was removed from the sweep gas on the third day and the drop of the $CO_2$ conversion was again observed, reaching the same value obtained during the first 24 h. As future targets, longer stability tests should be addressed for the evaluation of both, catalyst and membrane performance, in order to approach an industrial scenario.

To conclude, the implementation of a novel polymeric gas-separation membrane for *in-situ* water removal prevents the catalyst deactivation, and boosts the reaction kinetics. In addition, it was confirmed that these membranes are able to operate continuously at unprecedented high temperatures, above 250 °C exhibiting a good performance.

**Conflicts of interest**

There are no conflicts to declare.

**Acknowledgements**

This work was financially supported by the Spanish Government (SVP-2014-068356, SVP-2014-068713, RTI2018-102161 and IJCI-2016-28330 grants) and Generalitat Valenciana (PROMETEO/2018/006 grant).

The authors want also to acknowledge the Electron Microscopy Service from the Universitat Politècnica de València for their support in the SEM and TEM analysis performed in this work.

**References**

(1) Chi, Y.; Zhang, Y.; Li, G.; Zhang, Q.; Zhao, C.; Liu, S.; Yuan, L.; Liu, S.; Song, Y. CO2/CH4 Adsorption Property on Shale from China for ESGR Operation. *Energy Procedia* **2019**, *158*, 5396–5401. https://doi.org/https://doi.org/10.1016/j.egypro.2019.01.624.

(2) Hu, B.; Guild, C.; Suib, S. L. Thermal, Electrochemical, and Photochemical Conversion of CO2 to Fuels and Value-Added Products. *J. CO2 Util.* **2013**, *1*, 18–27. https://doi.org/https://doi.org/10.1016/j.jcou.2013.03.004.

(3) Change, U. N. F. C. on C. No Title http://unfccc.int/paris_agreement/items/9485.php.

(4) Sabatier P, S. J.-B. Comptes Rendus Des Séances De L'Académie Des Sciences, Section VI – Chimie. *Paris Impr. Gauthier-Villars* **1902**.

(5) Er-rbib, H.; Bouallou, C. Methanation Catalytic Reactor. *Comptes Rendus Chim.* **2014**, *17* (7), 701–706. https://doi.org/https://doi.org/10.1016/j.crci.2014.01.016.

(6) Su, X.; Xu, J.; Liang, B.; Duan, H.; Hou, B.; Huang, Y. Catalytic Carbon Dioxide Hydrogenation to Methane: A Review of Recent Studies. *J. Energy Chem.* **2016**, *25* (4), 553–565. https://doi.org/https://doi.org/10.1016/j.jechem.2016.03.009.

(7) Bailera, M.; Lisbona, P.; Romeo, L. M.; Espatolero, S. Power to Gas Projects Review: Lab,

Pilot and Demo Plants for Storing Renewable Energy and CO2. *Renew. Sustain. Energy Rev.* **2017**, *69*, 292–312. https://doi.org/https://doi.org/10.1016/j.rser.2016.11.130.
(8) Aziz, M. A. A.; Jalil, A. A.; Triwahyono, S.; Ahmad, A. CO2 Methanation over Heterogeneous Catalysts: Recent Progress and Future Prospects. *Green Chem.* **2015**, *17* (5), 2647–2663. https://doi.org/10.1039/C5GC00119F.
(9) Rönsch, S.; Schneider, J.; Matthischke, S.; Schlüter, M.; Götz, M.; Lefebvre, J.; Prabhakaran, P.; Bajohr, S. Review on Methanation – From Fundamentals to Current Projects. *Fuel* **2016**, *166*, 276–296. https://doi.org/https://doi.org/10.1016/j.fuel.2015.10.111.
(10) Garbarino, G.; Bellotti, D.; Riani, P.; Magistri, L.; Busca, G. Methanation of Carbon Dioxide on Ru/Al2O3 and Ni/Al2O3 Catalysts at Atmospheric Pressure: Catalysts Activation, Behaviour and Stability. *Int. J. Hydrogen Energy* **2015**, *40* (30), 9171–9182. https://doi.org/https://doi.org/10.1016/j.ijhydene.2015.05.059.
(11) Li, W.; Wang, H.; Jiang, X.; Zhu, J.; Liu, Z.; Guo, X.; Song, C. A Short Review of Recent Advances in CO2 Hydrogenation to Hydrocarbons over Heterogeneous Catalysts. *RSC Adv.* **2018**, *8* (14), 7651–7669. https://doi.org/10.1039/C7RA13546G.
(12) Tada, S.; Shimizu, T.; Kameyama, H.; Haneda, T.; Kikuchi, R. Ni/CeO2 Catalysts with High CO2 Methanation Activity and High CH4 Selectivity at Low Temperatures. *Int. J. Hydrogen Energy* **2012**, *37* (7), 5527–5531. https://doi.org/https://doi.org/10.1016/j.ijhydene.2011.12.122.
(13) Liu, J.; Li, C.; Wang, F.; He, S.; Chen, H.; Zhao, Y.; Wei, M.; Evans, D. G.; Duan, X. Enhanced Low-Temperature Activity of CO2 Methanation over Highly-Dispersed Ni/TiO2 Catalyst. *Catal. Sci. Technol.* **2013**, *3* (10), 2627–2633. https://doi.org/10.1039/C3CY00355H.
(14) Wang, W.; Wang, S.; Ma, X.; Gong, J. Recent Advances in Catalytic Hydrogenation of Carbon Dioxide. *Chem. Soc. Rev.* **2011**, *40* (7), 3703–3727. https://doi.org/10.1039/C1CS15008A.
(15) Miao, B.; Ma, S. S. K.; Wang, X.; Su, H.; Chan, S. H. Catalysis Mechanisms of CO2 and CO Methanation. *Catal. Sci. Technol.* **2016**, *6* (12), 4048–4058. https://doi.org/10.1039/C6CY00478D.
(16) Ocampo, F.; Louis, B.; Kiwi-Minsker, L.; Roger, A.-C. Effect of Ce/Zr Composition and Noble Metal Promotion on Nickel Based CexZr1−xO2 Catalysts for Carbon Dioxide Methanation. *Appl. Catal. A Gen.* **2011**, *392* (1), 36–44. https://doi.org/https://doi.org/10.1016/j.apcata.2010.10.025.
(17) Arandiyan, H.; Wang, Y.; Scott, J.; Mesgari, S.; Dai, H.; Amal, R. In Situ Exsolution of Bimetallic Rh–Ni Nanoalloys: A Highly Efficient Catalyst for CO2 Methanation. *ACS Appl. Mater. Interfaces* **2018**, *10* (19), 16352–16357. https://doi.org/10.1021/acsami.8b00889.
(18) Valinejad Moghaddam, S.; Rezaei, M.; Meshkani, F.; Daroughegi, R. Carbon Dioxide Methanation over Ni-M/Al2O3 (M: Fe, CO, Zr, La and Cu) Catalysts Synthesized Using the One-Pot Sol-Gel Synthesis Method. *Int. J. Hydrogen Energy* **2018**, *43* (34), 16522–16533. https://doi.org/https://doi.org/10.1016/j.ijhydene.2018.07.013.
(19) Duan, X.; Qian, G.; Zhou, X.; Sui, Z.; Chen, D.; Yuan, W. Tuning the Size and Shape of Fe Nanoparticles on Carbon Nanofibers for Catalytic Ammonia Decomposition. *Appl. Catal. B Environ.* **2011**, *101* (3), 189–196. https://doi.org/https://doi.org/10.1016/j.apcatb.2010.09.017.
(20) Hwang, S.; Lee, J.; Hong, U. G.; Seo, J. G.; Jung, J. C.; Koh, D. J.; Lim, H.; Byun, C.; Song, I. K. Methane Production from Carbon Monoxide and Hydrogen over Nickel–Alumina Xerogel Catalyst: Effect of Nickel Content. *J. Ind. Eng. Chem.* **2011**, *17* (1), 154–157. https://doi.org/https://doi.org/10.1016/j.jiec.2010.12.015.
(21) Hwang, S.; Lee, J.; Hong, U. G.; Baik, J. H.; Koh, D. J.; Lim, H.; Song, I. K. Methanation of Carbon Dioxide over Mesoporous Ni–Fe–Ru–Al2O3 Xerogel Catalysts: Effect of

Ruthenium Content. *J. Ind. Eng. Chem.* **2013**, *19* (2), 698–703. https://doi.org/https://doi.org/10.1016/j.jiec.2012.10.007.
(22) Petala, A.; Panagiotopoulou, P. Methanation of CO2 over Alkali-Promoted Ru/TiO2 Catalysts: I. Effect of Alkali Additives on Catalytic Activity and Selectivity. *Appl. Catal. B Environ.* **2018**, *224*, 919–927. https://doi.org/https://doi.org/10.1016/j.apcatb.2017.11.048.
(23) Delmelle Duarte, R. B., Franken, T., Burnat, D., Holzer, L., Borgschulte, A., & Heel, A., R. Development of Improved Nickel Catalysts for Sorption Enhanced CO2 Methanation. *Int. J. Hydrogen Energy* **2016**, *41* (44), 20185–20191. https://doi.org/https://doi.org/10.1016/j.ijhydene.2016.09.045.
(24) Agirre, I.; Acha, E.; Cambra, J. F.; Barrio, V. L. Water Sorption Enhanced CO2 Methanation Process: Optimization of Reaction Conditions and Study of Various Sorbents. *Chem. Eng. Sci.* **2021**, *237*, 116546. https://doi.org/10.1016/j.ces.2021.116546.
(25) Diban, N.; Aguayo, A. T.; Bilbao, J.; Urtiaga, A.; Ortiz, I. Membrane Reactors for in Situ Water Removal: A Review of Applications. *Ind. Eng. Chem. Res.* **2013**, *52* (31), 10342–10354. https://doi.org/10.1021/ie3029625.
(26) Borgschulte, A.; Gallandat, N.; Probst, B.; Suter, R.; Callini, E.; Ferri, D.; Arroyo, Y.; Erni, R.; Geerlings, H.; Züttel, A. Sorption Enhanced CO2 Methanation. *Phys. Chem. Chem. Phys.* **2013**, *15* (24), 9620–9625. https://doi.org/10.1039/C3CP51408K.
(27) Baker, R. W. *Membrane Technology and Applications*, 3rd ed.; Wiley, 2012.
(28) Fried, J. R. Basic Principles of Membrane Technology By Marcel Mulder (University of Twente, The Netherlands). Kluwer Academic: Dordrecht. 1996. 564 Pp. $255.00. ISBN 0-7823-4247-X. *J. Am. Chem. Soc.* **1997**, *119* (36), 8582. https://doi.org/10.1021/ja975504k.
(29) Morejudo, S. H.; Zanón, R.; Escolástico, S.; Yuste-Tirados, I.; Malerød-Fjeld, H.; Vestre, P. K.; Coors, W. G.; Martínez, A.; Norby, T.; Serra, J. M.; Kjølseth, C. Direct Conversion of Methane to Aromatics in a Catalytic Co-Ionic Membrane Reactor. *Science (80-. ).* **2016**, *353* (6299), 563–566. https://doi.org/10.1126/science.aag0274.
(30) Duan, C.; Huang, J.; Sullivan, N.; O'Hayre, R. Proton-Conducting Oxides for Energy Conversion and Storage. *Appl. Phys. Rev.* **2020**, *7* (1). https://doi.org/10.1063/1.5135319.
(31) Malerød-Fjeld, H.; Clark, D.; Yuste-Tirados, I.; Zanón, R.; Catalán-Martinez, D.; Beeaff, D.; Morejudo, S. H.; Vestre, P. K.; Norby, T.; Haugsrud, R.; Serra, J. M.; Kjølseth, C. Thermo-Electrochemical Production of Compressed Hydrogen from Methane with near-Zero Energy Loss. *Nat. Energy* **2017**, *2* (12), 923–931. https://doi.org/10.1038/s41560-017-0029-4.
(32) Escorihuela, S.; Toldra-Reig, F.; Escolástico, S.; Murciano, R.; Martínez, A.; Serra, J. M. Copper Surface-Alloying of H2-Permeable Pd-Based Membrane for Integration in Fischer–Tropsch Synthesis Reactors. *J. Memb. Sci.* **2021**, *619*. https://doi.org/10.1016/j.memsci.2020.118516.
(33) Ishikawa, H.; Kurose, K.; Murakami, T.; Ishii, T.; Hikita, H. A Membrane Reactor Capable of Shifting Equilibria in Reversible Reactions. *membrane* **1989**, *14*, 196–204. https://doi.org/10.5360/membrane.14.196.
(34) Rezai, S. A. S.; Traa, Y. Equilibrium Shift in Membrane Reactors: A Thermodynamic Analysis of the Dehydrogenative Conversion of Alkanes. *J. Memb. Sci.* **2008**, *319* (1), 279–285. https://doi.org/https://doi.org/10.1016/j.memsci.2008.03.051.
(35) Sánchez-Laínez, J.; Zornoza, B.; Carta, M.; Malpass-Evans, R.; McKeown, N. B.; Téllez, C.; Coronas, J. Hydrogen Separation at High Temperature with Dense and Asymmetric Membranes Based on PIM-EA(H2)-TB/PBI Blends. *Ind. Eng. Chem. Res.* **2018**, *57* (49), 16909–16916. https://doi.org/10.1021/acs.iecr.8b04209.
(36) Berchtold, K. A.; Singh, R. P.; Young, J. S.; Dudeck, K. W. Polybenzimidazole Composite

Membranes for High Temperature Synthesis Gas Separations. *J. Memb. Sci.* **2012**, *415–416*, 265–270. https://doi.org/10.1016/j.memsci.2012.05.005.
(37) Singh, R. P.; Dahe, G. J.; Dudeck, K. W.; Welch, C. F.; Berchtold, K. A. High Temperature Polybenzimidazole Hollow Fiber Membranes for Hydrogen Separation and Carbon Dioxide Capture from Synthesis Gas. In *Energy Procedia*; Elsevier Ltd, 2014; Vol. 63, pp 153–159. https://doi.org/10.1016/j.egypro.2014.11.015.
(38) Akhtar, F. H.; Vovushua, H.; Villalobos, L. F.; Shevate, R.; Kumar, M.; Nunes, S. P.; Schwingenschlögl, U.; Peinemann, K. V. Highways for Water Molecules: Interplay between Nanostructure and Water Vapor Transport in Block Copolymer Membranes. *J. Memb. Sci.* **2019**, *572*, 641–649. https://doi.org/10.1016/J.MEMSCI.2018.11.050.
(39) Knauth, P.; Hou, H.; Bloch, E.; Sgreccia, E.; Di Vona, M. L. Thermogravimetric Analysis of SPEEK Membranes: Thermal Stability, Degree of Sulfonation and Cross-Linking Reaction. *J. Anal. Appl. Pyrolysis* **2011**, *92* (2), 361–365. https://doi.org/10.1016/J.JAAP.2011.07.012.
(40) Asadi Tashvigh, A.; Chung, T. S. Robust Polybenzimidazole (PBI) Hollow Fiber Membranes for Organic Solvent Nanofiltration. *J. Memb. Sci.* **2019**, *572*, 580–587. https://doi.org/10.1016/j.memsci.2018.11.048.
(41) Singha, S.; Jana, T. Structure and Properties of Polybenzimidazole/Silica Nanocomposite Electrolyte Membrane: Influence of Organic/Inorganic Interface. **2014**. https://doi.org/10.1021/AM506260J.
(42) Pye, D. G.; Hoehn, H. H.; Panar, M. Measurement of Gas Permeability of Polymers. II. Apparatus for Determination of Permeabilities of Mixed Gases and Vapors. *J. Appl. Polym. Sci.* **1976**, *20* (2), 287–301. https://doi.org/doi:10.1002/app.1976.070200201.
(43) Hoehn, H. H. Aromatic Polyamide Membranes. In *Materials Science of Synthetic Membranes*; American Chemical Society, 1985; Vol. 269, pp 81–98. https://doi.org/doi:10.1021/bk-1985-0269.ch00410.1021/bk-1985-0269.ch004.
(44) Alexander Stern, S. Polymers for Gas Separations: The next Decade. *J. Memb. Sci.* **1994**, *94* (1), 1–65. https://doi.org/https://doi.org/10.1016/0376-7388(94)00141-3.
(45) Poley, L. H.; da Silva, M. G.; Vargas, H.; Siqueira, M. O.; Sánchez, R. Water and Vapor Permeability at Different Temperatures of Poly (3-Hydroxybutyrate) Dense Membranes. *Polímeros Ciência e Tecnol.* **2005**, *15* (1), 22–26.
(46) Gülmüs, S. A.; Yilmaz, L. Effect of Temperature and Membrane Preparation Parameters on Gas Permeation Properties of Polymethacrylates. *J. Polym. Sci. Part B Polym. Phys.* **2007**, *45* (22), 3025–3033. https://doi.org/doi:10.1002/polb.21258.
(47) Komatsuka, T.; Nagai, K. Temperature Dependence on Gas Permeability and Permselectivity of Poly(Lactic Acid) Blend Membranes. *Polym. J.* **2009**, *41*, 455. https://doi.org/10.1295/polymj.PJ2008266.
(48) Zhukova, E. K.; Kuznetsov, A. A.; Yablokova, M. Y.; Alentiev, A. Y. Gas Separation Properties of New Thermoplastic Polyimides with Phenylamide Groups in Diamine Moiety: Effect of Polymer Structure. *Pet. Chem.* **2014**, *54* (7), 544–550. https://doi.org/10.1134/s0965544114070159.
(49) Guzmán-Lucero, D.; Palomeque-Santiago, J.; Camacho-Zúñiga, C.; Ruiz-Treviño, F.; Guzmán, J.; Galicia-Aguilar, A.; Aguilar-Lugo, C. Gas Permeation Properties of Soluble Aromatic Polyimides Based on 4-Fluoro-4,4'-Diaminotriphenylmethane. *Materials (Basel).* **2015**, *8* (4), 1951.
(50) Escorihuela, S.; Valero, L.; Tena, A.; Shishatskiy, S.; Escolástico, S.; Brinkmann, T.; Serra, J. Study of the Effect of Inorganic Particles on the Gas Transport Properties of Glassy Polyimides for Selective CO2 and H2O Separation. *Membranes (Basel).* **2018**, *8* (4), 128.
(51) Onda, A.; Hara, S.; Kajiyoshi, K.; Yanagisawa, K. Synthesis of Manganese Oxide Octahedral Molecular Sieves Containing Cobalt, Nickel, or Magnesium, and the Catalytic Properties for Hydration of Acrylonitrile. *Appl. Catal. A Gen.* **2007**, *321* (1), 71–78. https://doi.org/https://doi.org/10.1016/j.apcata.2007.01.037.

(52) Suib, S. L. Structure, Porosity, and Redox in Porous Manganese Oxide Octahedral Layer and Molecular Sieve Materials. *J. Mater. Chem.* **2008**, *18* (14), 1623–1631. https://doi.org/10.1039/B714966M.

(53) Cerdá-Moreno, C.; Chica, A.; Keller, S.; Rautenberg, C.; Bentrup, U. Ni-Sepiolite and Ni-Todorokite as Efficient CO2 Methanation Catalysts: Mechanistic Insight by Operando DRIFTS. *Appl. Catal. B Environ.* **2020**, *264*, 118546. https://doi.org/https://doi.org/10.1016/j.apcatb.2019.118546.

(54) Gil, A.; Diaz, A.; Montes, M. Passivation and Reactivation of Nickel Catalysts. *J. Chem. Soc. Faraday Trans.* **1991**, *87* (5), 791–795. https://doi.org/10.1039/FT9918700791.

(55) Huber, F.; Yu, Z.; Lögdberg, S.; Rønning, M.; Chen, D.; Venvik, H.; Holmen, A. Remarks on the Passivation of Reduced Cu-, Ni-, Fe-, Co-Based Catalysts. *Catal. Letters* **2006**, *110* (3), 211–220. https://doi.org/10.1007/s10562-006-0111-1.

(56) Tena, A.; Shishatskiy, S.; Meis, D.; Wind, J.; Filiz, V.; Abetz, V. Influence of the Composition and Imidization Route on the Chain Packing and Gas Separation Properties of Fluorinated Copolyimides. *Macromolecules* **2017**, *50* (15), 5839–5849. https://doi.org/10.1021/acs.macromol.7b01051.

(57) Escorihuela, S.; Tena, A.; Shishatskiy, S.; Escolástico, S.; Brinkmann, T.; Serra, J.; Abetz, V. Gas Separation Properties of Polyimide Thin Films on Ceramic Supports for High Temperature Applications. *Membranes (Basel).* **2018**, *8* (1), 16.

(58) Weigelt, F.; Escorihuela, S.; Descalzo, A.; Tena, A.; Escolástico, S.; Shishatskiy, S.; Serra, J. M.; Brinkmann, T. Novel Polymeric Thin-Film Composite Membranes for High-Temperature Gas Separations. *Membranes (Basel).* **2019**, *9* (4), 51.

(59) Massa, F.; Coppola, A.; Scala, F. A Thermodynamic Study of Sorption-Enhanced CO2 Methanation at Low Pressure. *J. CO2 Util.* **2020**, *35*, 176–184. https://doi.org/10.1016/j.jcou.2019.09.014.

(60) Mebrahtu, C.; Perathoner, S.; Giorgianni, G.; Chen, S.; Centi, G.; Krebs, F.; Palkovits, R.; Abate, S. Deactivation Mechanism of Hydrotalcite-Derived Ni-AlO: X Catalysts during Low-Temperature CO2 Methanation via Ni-Hydroxide Formation and the Role of Fe in Limiting This Effect. *Catal. Sci. Technol.* **2019**, *9* (15), 4023–4035. https://doi.org/10.1039/c9cy00744j.

(61) Yao, X.; Zhang, Y.; Du, L.; Liu, J.; Yao, J. Review of the Applications of Microreactors. *Renewable and Sustainable Energy Reviews*. Elsevier Ltd July 1, 2015, pp 519–539. https://doi.org/10.1016/j.rser.2015.03.078.